VISCOUS VORTEX FLOWS

R. P. Weston, J. P. Chamberlain,
C. H. Liu, and Peter-Michael Hartwich*
NASA Langley Research Center
Hampton, Virginia

*NRC - NASA Resident Research Associate

INTRODUCTION

Several computational studies are currently being pursued that focus on various aspects of representing the entire lifetime of the viscous trailing vortex wakes generated by an aircraft. The computational regions are indicated in the figure below, with the vicinity around the vortex-generating aircraft designated as region A. The formation and subsequent near-wing development of the leading-edge vortices formed by a delta wing are being calculated at modest Reynolds numbers using a three-dimensional, time-dependent Navier-Stokes code. The calculations exhibit realistic vortex characteristics including behavior similar to vortex bursting at high angles of attack. Another computer code has been developed to focus on the roll-up, the trajectory, and the mutual interaction of the trailing vortices further downstream from the wing (region B) using a two-dimensional, time-dependent Navier-Stokes algorithm. This code has also been used to study the modification of the vortex behavior due to ground-proximity effects and the enhanced vortex decay induced by atmospheric temperature gradients. To investigate the effect of a cross-wind ground shear flow on the drift and decay of the far-field trailing vortices (region C), yet another code has been developed that employs Euler equations along with matched asymptotic solutions for the decaying vortex filaments. And finally, to simulate the conditions far downstream after the onset of the Crow instability in the vortex wake (region D), a full three-dimensional, time-dependent Navier-Stokes code has been developed to study the behavior of interacting vortex rings.

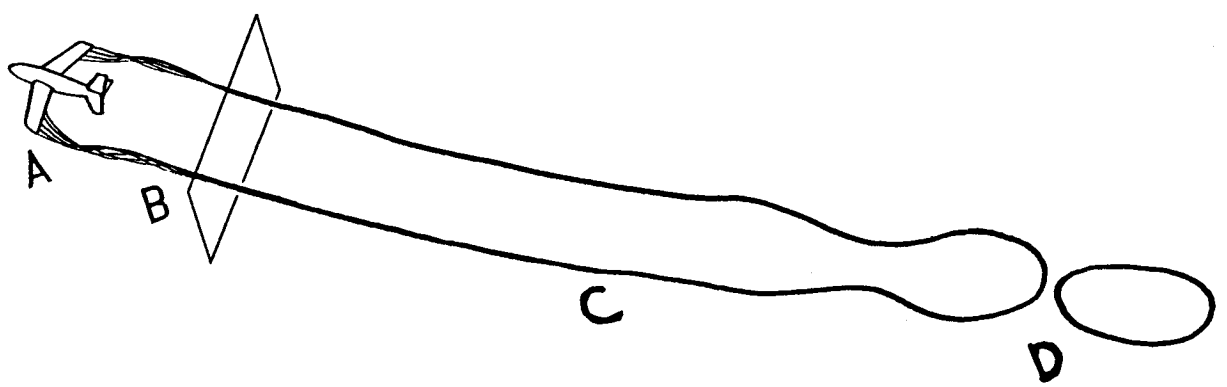

3-D NAVIER-STOKES CALCULATIONS

The formation and the subsequent near-wing development of the leading-edge vortices formed by a delta wing are simulated by time-accurate finite-difference solutions to the Navier-Stokes equations for three-dimensional, incompressible flows with moderate Reynolds numbers. This particular aspect of an extensive numerical study of vortex flow fields generated by aircraft was chosen because a broad experimental data base allows thorough evaluation of the numerical results. The discretized momentum equations are integrated by an Euler-explicit, time-marching procedure that is first and second-order accurate in time and space, respectively. The pressure field is computed simultaneously by a simplified Jacobi method applied to the Poisson equation for the pressure. Truly transient solutions are achieved by repeating the iterative procedure as with time level until the flow is source free.

- Body-fitted coordinates
- Incompressible
- Time-dependent
- Explicit finite-difference

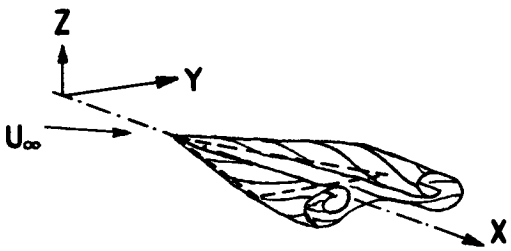

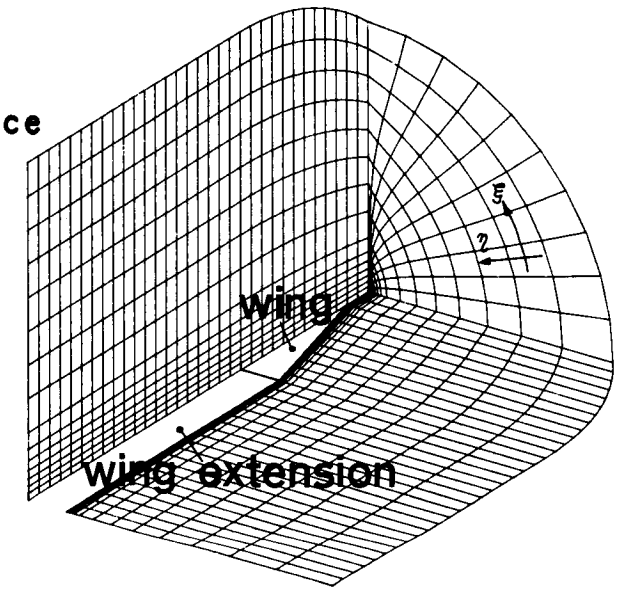

COMPARISON WITH EXPERIMENT AT $\alpha = 20.5^{\circ}$

This figure shows a comparison of streamline patterns that were determined from the velocity fields as steady-state solutions to the Navier-Stokes equations (Re = 250 and Re = 1500) and to the Euler equations (Re $\rightarrow \infty$), and also those that were photographed in a water tunnel (Re = 900). In all four cases the lateral deviations of the vortex streamlines are quite similar. The circumferential velocities of the experimentally observed vortices are judged to be greater than those in the computed flow fields since the number of coils per axial length in the photograph is higher than in the computations. The values for κ give an estimation of the additional numerical viscosity which has to be added to numerically stabilize the finite-difference solutions of the Navier-Stokes equations (Re = 1500) and of the Euler equations (Re $\rightarrow \infty$). The quantity κ can be interpreted as the reciprocal of a Reynolds number, giving the effective Reynolds number during the computations as $(\frac{1}{Re})_{effective} = (\frac{1}{Re})_{nominal} + \kappa$.

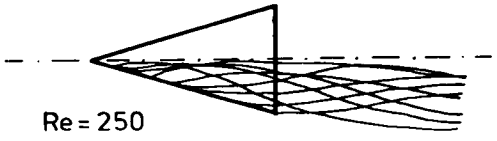

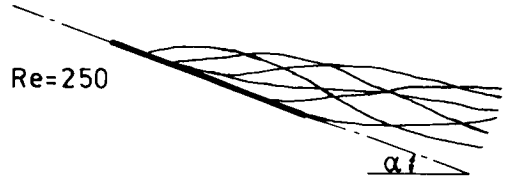

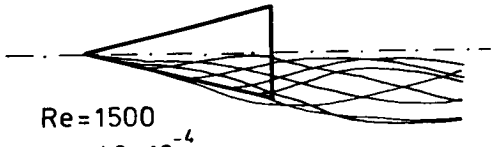

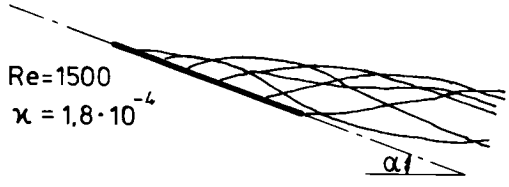

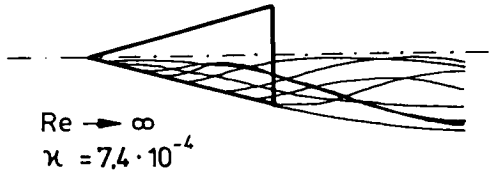

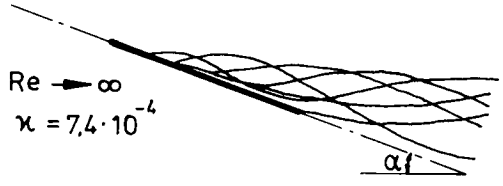

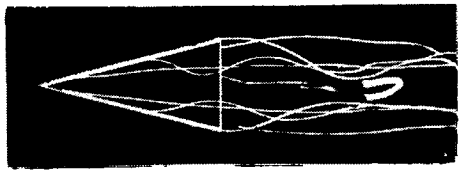

Re=900 experiment

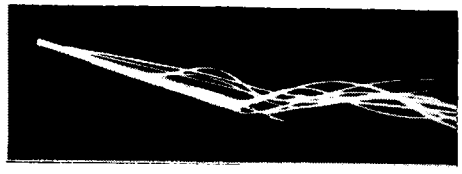

Re=900 experiment

VELOCITY FIELD FOR 78.6% CHORD, $\alpha = 20.5^{\circ}$

This figure shows the projections of the velocities in planes which intersect the delta wing perpendicularly at 78.6% of the root chord. The aspect ratio is AR = 1 and the angle of attack is 20.5 degrees. The velocity fields represent steady-state solutions to the Navier-Stokes equations (Re = 250 and Re = 1500) and to the Euler equations (Re $\rightarrow \infty$). For Re = 250, no additional numerical damping was necessary, whereas numerically stable solutions for Re = 1500 and Re $\rightarrow \infty$ were obtained only after additional damping, indicated by κ, has been introduced in the discretized momentum equations. The vortex for Re = 250 lies higher and closer to the plane of symmetry than in the other two cases. The velocity distributions for Re = 1500 and Re $\rightarrow \infty$ look quite similar if a small region in the neighborhood of the wing is neglected where the different boundary conditions for viscous and inviscid flows affect the solution. The small size of this region suggests that for the computation of vortex flows around sharp-edged delta wings with Re > $0(10^3)$ the friction forces may be neglected. To provide further evidence for this conclusion, additional investigations are in progress.

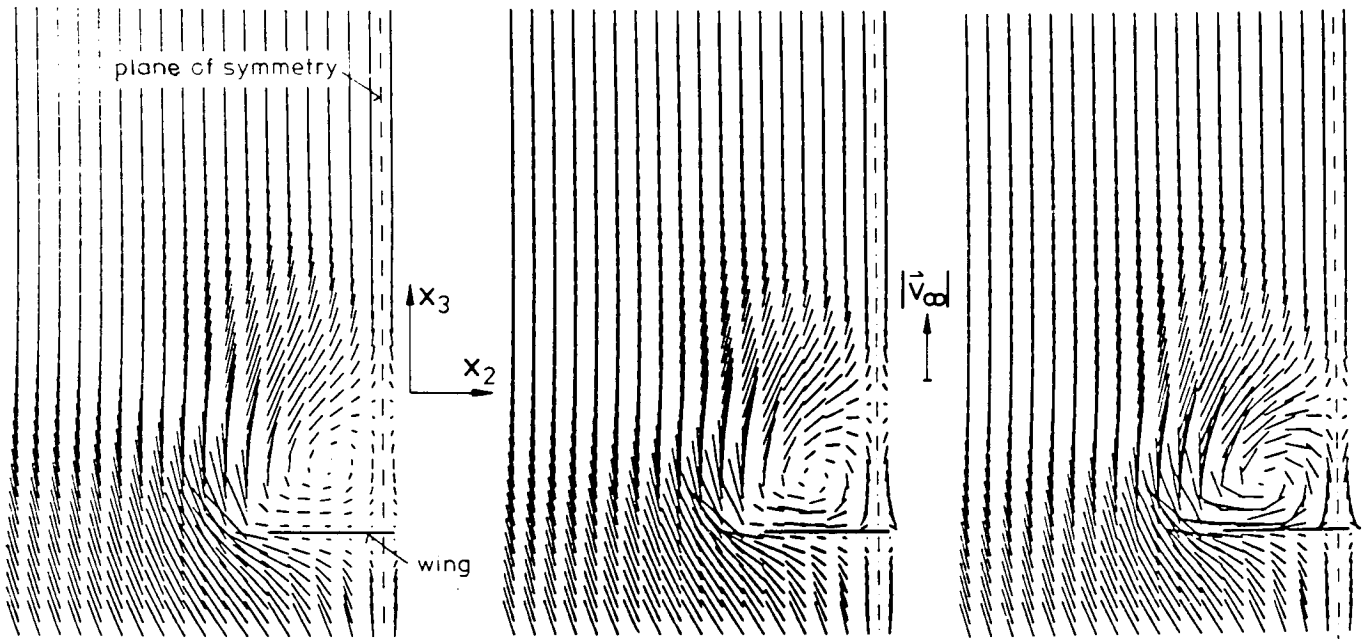

TWO-DIMENSIONAL INITIAL VALUE PROBLEM

The governing equations are expressed in terms of the variables of stream function (ψ) and vorticity (ω). The equation of continuity can then be cast as a Poisson equation and the curl of the momentum equation becomes the vorticity transport equation, where t is time, ν is the kinematic viscosity, and v and w are the velocity components in the y and z directions, respectively. The subscripts denote partial derivatives. The initial vorticity distribution provides the initial condition and the boundary condition for the unbounded flow is based on the fact that the vorticity distribution is confined to one area and decays exponentially with distance from that area. The exact solution for the Poisson equation is given by the Biot-Savart law. However, the computation of the boundary conditions using this law directly is extremely expensive. A considerable time savings can be achieved by expanding the Biot-Savart integral in a power series in terms of vorticity. The coefficients of the terms in the power series are moments of the vorticity distribution. Previous studies have shown that the first moments and several linear combinations of higher moments are time invariant. These results can be used to determine the boundary condition for the numerical calculations and are also used in checking the accuracy of the numerical solutions as they proceed.

Incompressible, Navier-Stokes Eqns.

Continuity: $\nabla \cdot \vec{V} = 0 \Rightarrow \Delta \psi = -\omega$ (Poisson eqn)

Vorticity Transport : $\omega_t + v\,\omega_y + w\,\omega_z = \nu\,\Delta\,\omega$

I.C. $\omega(\vec{x},0) = \omega_o(\vec{x})$

B.C. $\omega(x,t) \to 0$ exponentially as $x \to \infty$

Boundary values of ψ are evaluated using a moment expansion of the Biot-Savart law

FLOWCHART

The basic algorithm performed by the program is outlined below:

1. The volume integrals are evaluated using Simpson integration over the computational domain. The time varying integrals are evaluated at each time step, while the time-invariant integrals are evaluated initially and then only periodically to monitor the accuracy of the solution.

2. The results from step one are used to obtain the expansion coefficients which are in turn used to determine values of ψ at the boundary.

3. A fast Poisson solver is used to determine the values of ψ in the interior of the computational domain. The solver currently in use is a direct method developed by the National Center for Atmospheric Research (NCAR). The method uses a finite-difference formulation and is second-order accurate in the spatial directions.

4. The velocity field is obtained by using second-order centered differences to obtain the curl of ψ. The velocity values are written over the stream function values to minimize the required computer storage.

5. The vorticity field is advanced in time by using a finite-difference representation of the vorticity transport equation. The program currently uses the Dufort-Frankel method (ref. 1) for solving the vorticity transport equation; this explicit method is accurate to $O[(\Delta t)^2, (\Delta x_i)^2, \nu(\Delta t/\Delta x_i)^2;\ i = 1, 2, 3]$. Explicit methods for solving the vorticity transport equation appear to be more appropriate than implicit methods in this case.

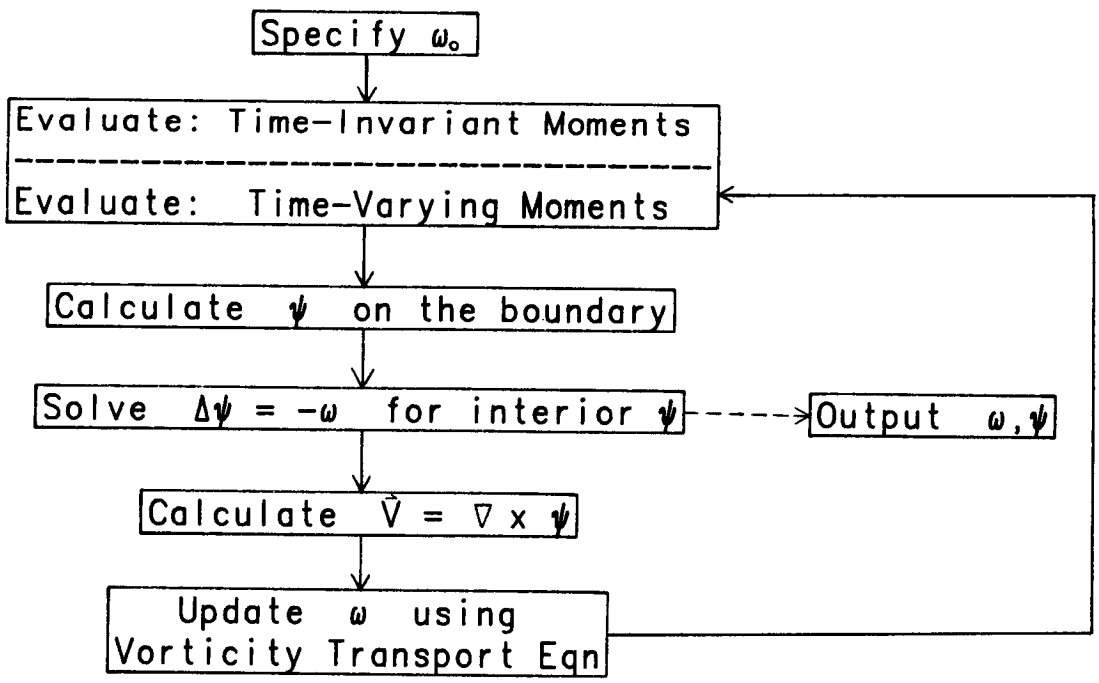

EVOLUTION OF VORTICITY FOR SPANLOAD OF TRANSPORT IN LANDING CONFIGURATION

This figure displays the resultant contours of vorticity for successive planes downstream of the wing. The calculations were performed at a Reynolds number (Γ/ν) of 20,000. The results are shown for only the right half-plane since the flow is assumed to exhibit mirror symmetry about the line y = 0. Since the computational grid follows the vortices, the projection of the wing trailing edge appears as the horizontal line that rises in successive planes.

The example is for a spanload distribution like that obtained with a transport aircraft using flaps on landing or takeoff. The resulting initial vorticity distribution has been simplified by distributing the vorticity along a horizontal line, unlike the more complicated positions expected in reality. Note the negative vorticity values associated with the reduction in lift around the fuselage-wing junction.

Successive frames illustrate the evolution of the vortex system in time and demonstrate the ultimate merging of the vortices from the wing tip and flap tip. A movie generated from these calculations has been useful in observing the progress of these vortex interactions.

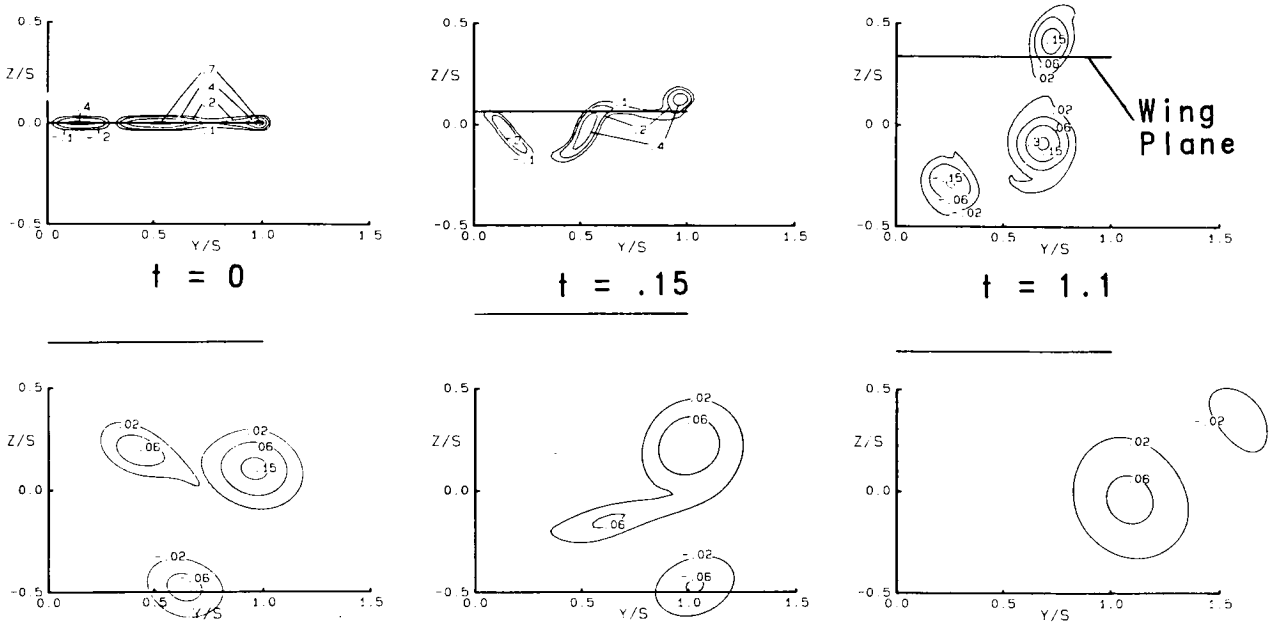

INTERACTION OF DECAYING TRAILING VORTICES IN SPANWISE SHEAR FLOW

The drift of trailing vortices in a crosswind near to the ground is modeled by an unsteady, two-dimensional, rotational flow field with a concentration of large vorticity in spots having a finite but small effective size and finite total strength. The problem is analyzed by a combination of the method of matched asymptotic analyses for the decay of the vortical spots and the Euler solution for the unsteady rotational flow. Using the method of averaging, a numerical scheme is developed in which the grid size and time step depend only on the length and velocity scales of the background flow and are independent of the effective core size of a vortical spot. The core size can be much smaller than the grid size while the peak velocity in the core is inversely proportional to the spot size. Numerical results are presented to demonstrate the strong interaction between the trajectories of the vortical spots and the redistribution of vorticity in the background flow field (ref. 2).

COORDINATE TRANSFORMATION

The problem of a steady far-wake vortex can be simplified by reducing the problem to an equivalent unsteady two-dimensional problem in a plane normal to the flight direction. This simplification is performed by changing the coordinate z to a time variable t using $z=z^*-W_\infty t$, where z is stationary and z^* points in the downstream direction and moves with the airplane at velocity W_∞ (see figure). This assumption ignores the streamwise curvature of the trailing vortex filaments, their initiation at the trailing edge, and the variation of the velocity parallel to the z axis. Mathematically, we assume that $d/dz \ll d/dx$ and d/dy with x,y as the span and vertical direction, respectively. In the x-y plane at a station z, the trailing vortices are represented by "vortex spots" of small effective size inside of which there is a strong vorticity distribution with finite total strength.

This model is employed to study the drift and decay of farfield trailing vortices (vortical spots) in a cross wind (a spanwise shear flow) near the ground.

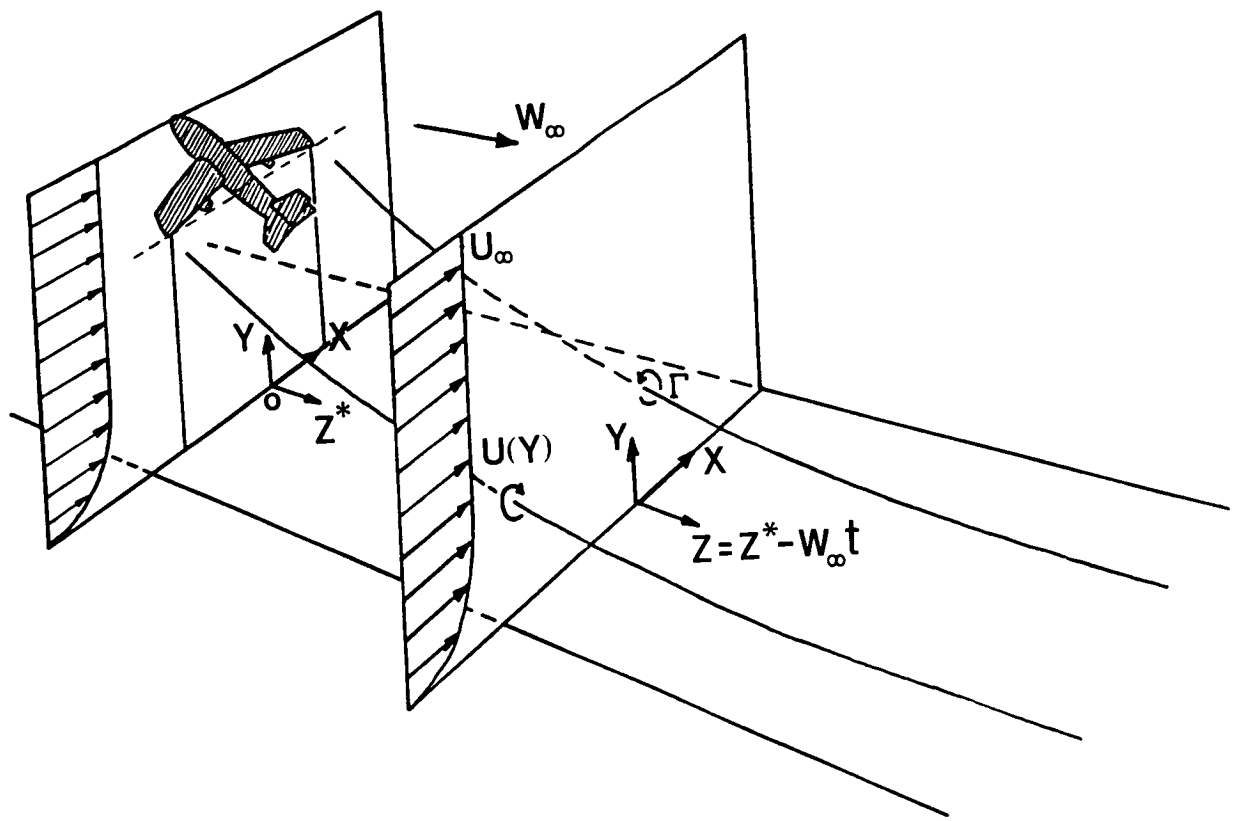

EFFECT OF VORTEX STRENGTH ON TRAJECTORY

To gain a qualitative understanding of the interaction of vortical spots with a background shear flow, we study first the case of a single vortical spot. This figure shows the trajectories of a single concentrated decaying vortical spot of various strengths submerged in a background shear flow. The initial vertical position of the spot is at y=1 and the initial background shear flow is chosen as $U_0(y)=1-e^{-y}$. The results show that the vortical spots with positive circulation drift downstream and upward while the vortical spots with negative circulation drift downstream and downward but eventually turn backward (t>t*). This phenomenon is more pronounced as the strength of the vortical spot increases. To explain this phenomenon we consider the case of a single vortical spot with $\Gamma>0$. The disturbed flow moves downward behind the spot, x<X, and upward ahead of the spot, x>X. For an initial background vorticity ω_0 with $\omega_0'(y) >0$, the disturbed flow increases the vorticity behind the spot and decreases the vorticity ahead of it, i.e., $\tilde{\zeta}>0$ for x<X and $\tilde{\zeta}<0$ for x>X. The background vorticity variation $\tilde{\zeta}$ in turn induces an upward motion of the vortical spot for $\Gamma>0$. From similar arguments, we can explain that the background vorticity variation $\tilde{\zeta}$ will induce a downward motion of the vortical spot with $\Gamma<0$. The reason that a vortical spot of negative strength turns around and drifts upstream as it gets closer and closer to the ground can be attributed to the decrease of the contribution of the background shear flow to the forward velocity of the spot and to the increase of the induced velocity by the image of the vortical spot with respect to the ground, y=0. It should be pointed out here once more that the vortical spot will drift horizontally when the background shear flow is either a uniform flow ($\omega_0=0$) or a constant shear flow (ω_0=constant) and there will be no change in the background flow, $\tilde{\zeta}\equiv 0$.

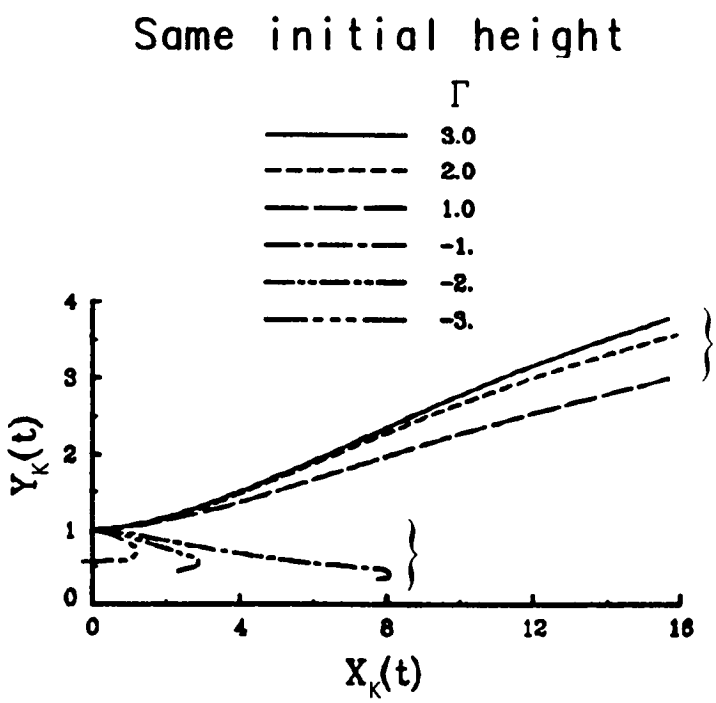

VORTICAL PAIRS SIMULATING TRAILING VORTICES IN A CROSSWIND

The trailing vortex wakes far downstream of an aircraft are modeled by a simple vortex pair whose vorticity distributions are concentrated and are centered at $(\mp X_k(0), Y_k(0))$ with strength $\mp\Gamma$ and effective vortical size $\delta(0)$. The goal of the following numerical examples is to simulate the interaction of the decaying trailing vortical pairs subjected to a cross-flow (spanwise) ground shear. The background shear flow used in the examples is an exponential profile.

In order to find out when we have to use the shear layer solution, we studied the trajectories of a pair of vortices in a shear layer for different initial vortex heights. The $Y_{R,min}$ approaches an asymptotic value of 2.6 when $Y_k(0)$ is greater than 7.0. This means that when the vortex spots are above y=7, they are far above the shear layer and the interaction with the shear layer is negligible. The corresponding trajectories (in real spanwise positions) of the vortical pair, starting at different heights $Y_k(0)$=1,2,3,4,5 in the shear layer, are displayed in this figure to show that the trajectories of the vortical spots are sensitive to the starting height, i.e., the altitude of the airplane relative to the thickness of the shear layer.

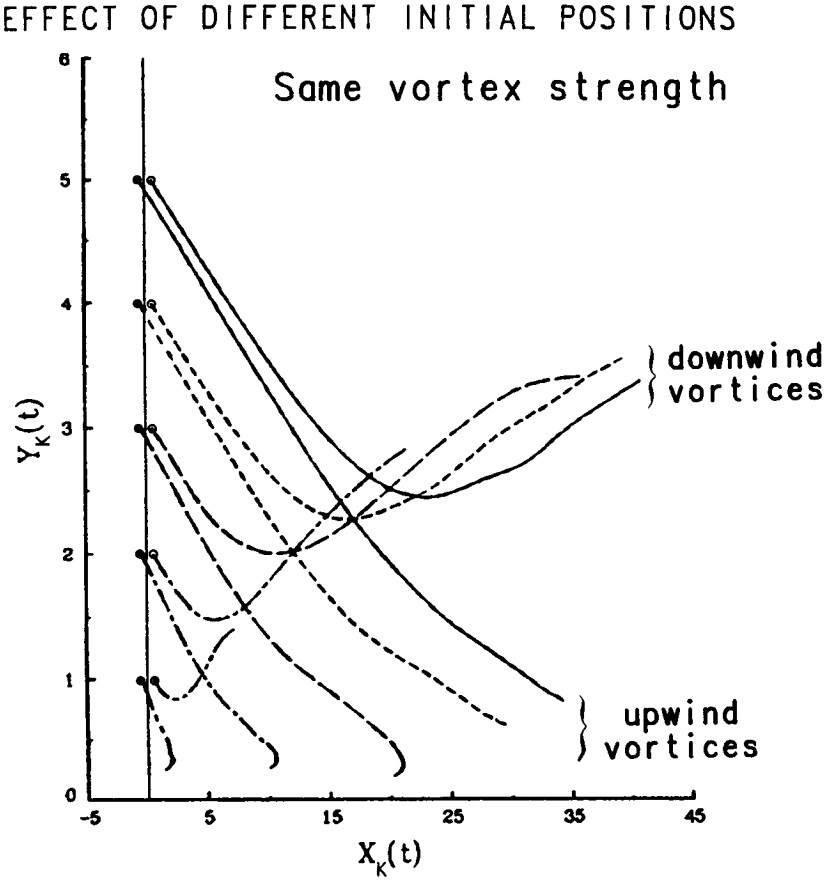

NAVIER-STOKES CALCULATIONS FOR UNSTEADY, THREE-DIMENSIONAL VORTEX-DOMINATED FLOWS

A finite-difference Navier-Stokes code has been developed for calculating unsteady, three-dimensional, vortex-dominated flows in unbounded fluid domains. The algorithm uses an improved boundary condition specification which allows the unbounded nature of the physical problem to be represented on a finite computational domain. This boundary condition specification permits the efficient computation of flows due to closed ring-like vortical tubes or structures. These structures are important elements in fluid flows such as free jets, atmospheric turbulence, and the far-field wakes of aircraft, and studies of their interaction may aid in an understanding of complex vortical fluid flows.

The primary variables used in the computations are the vorticity and the vector velocity potential, which is defined as a divergence-free vector field whose curl yields the velocity. This definition of the vector velocity potential automatically satisfies the incompressible continuity equation, and for unbounded flow relates the vector potential directly to the vorticity through an integral relationship (the vector Poisson integral). In theory, this integral relationship could be used to yield the velocity directly from the vorticity, but the numerical evaluation of the Poisson integral throughout the computational domain is very time consuming. The current algorithm avoids the expense of directly computing the integral by approximating the integral values at the domain boundary with a series representation, and then using these values along with a fast Poisson solver in the domain interior. This technique yields a fast, accurate solution for the velocity field of the unbounded-domain physical problem with a finite computational domain.

Incompressible, Laminar Flow

Continuity: $\nabla \cdot \vec{V} = 0 \Rightarrow \Delta \vec{A} = -\vec{\omega}$ (Poisson eqn)

Vorticity Transport : $\vec{\omega}_t = \nabla \times (\vec{V} \times \vec{\omega}) + \nu \Delta \vec{\omega}$

I.C. $\vec{\omega}(\vec{x},0) = \vec{\omega}_o(\vec{x})$

B.C. $\vec{\omega}(\vec{x},t) \to 0$ exponentially as $x \to \infty$

Boundary values of $\vec{A}$ are evaluated using a moment expansion of the Biot-Savart law

BOUNDARY CONDITION ACCURACY

The accuracy and efficiency of two approximate vector-potential boundary condition methods were evaluated by comparing them with an exact solution that used Poisson integral evaluations to generate the boundary conditions. The two approximate methods were the truncated series method mentioned in the previous figure and a method that enforces zero normal velocity at the boundary by setting $\vec{A}$ to zero at the boundary.

The vorticity distribution chosen for the boundary condition checks is shown in the upper right figure as a vorticity-magnitude isosurface. This distribution represents two Gaussian-core vortex rings with equal strengths, radii, and core diameters whose axes of symmetry lie in the x-y plane and cross the x-axis at an angle of ±22.5°. The centers of the rings lie on the y-axis at ±1.5 units, where a unit of length is the toroidal radius of each ring. The effective core radius (the radius at which the vorticity magnitude has fallen to 1/e of the maximum vorticity magnitude) is 0.5. The computational domain is a cube with edges of length 8 centered about the origin. This domain size is the practical minimum cubical size that will still enclose both vortical rings and thus represents a "worst-case" test condition.

The three boundary condition figures show contour plots of the magnitude of $\vec{A}$ in the x-y plane of the domain for each of the three boundary condition methods. It is evident from the figures that the finite solution domain affects both the series method and zero normal-velocity method solutions, although the series solution is not affected to nearly as great an extent. For slightly larger domains the series method solution closely approximates the Poisson method solution, whereas the global character of the zero normal-velocity solution is altered by the closed boundary.

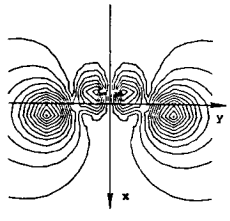

POISSON INTEGRAL B.C.'S

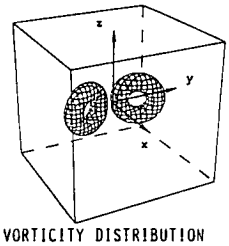

VORTICITY DISTRIBUTION

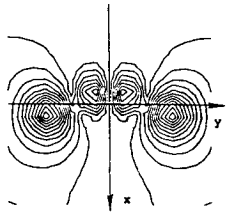

SERIES B.C.'S

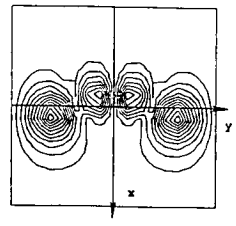

$|\vec{A}| = 0$ B.C.'S

MERGER OF VORTEX RING PAIR

This figure shows the oblique collision, merging, and deformation of two circular, Gaussian-core vortex rings. The first two plots show representative isosurfaces of the initial vorticity and vector velocity potential magnitudes, respectively, and the last four plots show the time development of the vector potential isosurface. The intersections on the surfaces represent grid point locations, and the cube represents the computational domain boundary. The rings collide and merge to form a single distorted oblong ring, which continues to deform until the major and minor axes have switched their orientation. This behavior has been observed experimentally, and work is currently in progress to further correlate the code results with experiment. It is hoped that this algorithm will be useful in understanding and analyzing the physics of vortex-dominated flows.

(VECTOR POTENTIAL STREAM SURFACES)

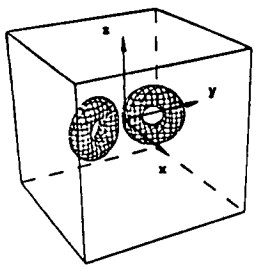

VORTICITY

$\tau = 0$

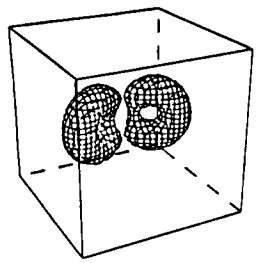

VECTOR POTENTIAL

$\tau = 0$

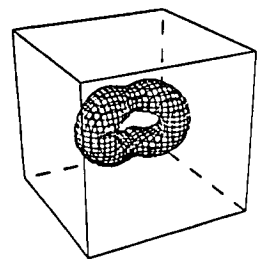

$\tau = 10.4$

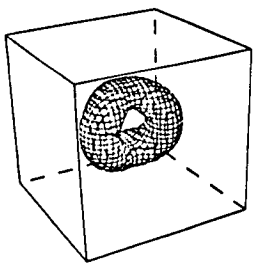

$\tau = 20.2$

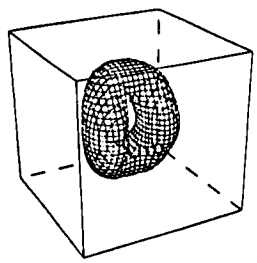

$\tau = 40.9$

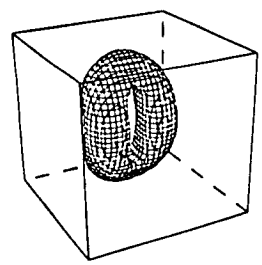

$\tau = 60.1$

REFERENCES

1. Dufort, E.C., and Frankel, S.P.: "Stability Conditions in the Numerical Treatment of Parabolic Differential Equations," Math. Tables and Other Aids to Computation, Vol. 7, 1953, pp. 135-152.

2. Liu, C. H. and Ting, L.: "Interaction of Decaying Trailing Vortices in Ground Shear," Proceedings of 4th International Conference on Applied Numerical Modeling, Tainan, Taiwan, Dec. 1984, pp. 646-655.